

Ultra-high pressure disordered eight-coordinated phase of Mg₂GeO₄: Analogue for super-Earth mantles

R. Dutta^{1,2*}, S. J. Tracy¹, J. Yang¹, P. C. Burnley³, D. Smith⁴, Y. Meng⁴, S. Chariton⁵, V. B. Prakapenka⁵, and T. S. Duffy²

¹Earth and Planets Laboratory, Carnegie Institution for Science, Washington DC 20015 USA.

²Department of Geosciences, Princeton University, Princeton, NJ 08540 USA.

³Department of Geoscience, University of Nevada, Las Vegas, NV 89154 USA.

⁴HPCAT, Advanced Photon Source, Argonne National Laboratory, Argonne, IL 60439 USA

⁵Center for Advanced Radiation Sources, University of Chicago, Chicago, IL 60637 USA.

Abstract

High-pressure phases of Mg₂GeO₄ have been explored as an analogue system for the ultra-high pressure behavior of Mg₂SiO₄. Using a laser-heated diamond anvil cell combined with *in situ* synchrotron X-ray diffraction, we have identified a novel phase in which germanium adopts eight-fold coordination with oxygen. The cubic Th₃P₄-type phase was synthesized upon heating Mg₂GeO₄ to ~1600 K at 162 GPa and it remained stable up to ~ 275 GPa and 2020 K. While the Th₃P₄-type phase is commonly observed in chalcogenides, it has not been reported before in any oxide composition. If applicable to silicates, the formation of this highly coordinated and intrinsically disordered phase or a closely related structure as suggested by theoretical calculations would have important implications for the interior mineralogy of large, rocky extrasolar planets.

Introduction

A large number of exoplanets have been discovered in recent years, including many planets whose mean density indicates they have rocky interiors that may be up to ten times more massive than the Earth (1). There is significant interest in understanding the mineralogy of the deep interiors of such bodies where the pressure at the core-mantle boundary is predicted to reach up to 1 TPa (2–4). Theoretical calculations suggest that silicate structures with partial or complete eight-fold coordination of silicon can be stabilized above 500 GPa (4). These pressures are expected to be

*Corresponding author: rdutta@carnegiescience.edu

reached within the mantles of rocky exoplanets of ~ 4 Earth masses or greater (3, 4). Phase changes with accompanying coordination changes may strongly affect the structure, dynamics, and heat flow in exoplanet interiors (1, 5). Unfortunately, the predicted pressures and temperatures of these transitions in silicates are beyond what can be accessed with current static compression techniques.

Germanates are known to be effective analogues for silicates as they undergo similar phase transitions but at lower pressures (6, 7). For example, the perovskite (Pv) to post-perovskite (pPv) transition occurs near 65 GPa in MgGeO_3 (8) as opposed to ~ 125 GPa in the corresponding silicate. Recently, theoretical calculations have examined ultra-high pressure transitions in the MgO-GeO_2 system and suggest that it can be an excellent analogue system for ultra-high pressure phase transitions in silicate minerals (9). These calculations predict that MgGeO_3 post-perovskite and MgO will combine to form an eight-coordinated tetragonal phase of Mg_2GeO_4 ($I\bar{4}2d$) at ~ 175 GPa (9) (Suppl. Material, Fig. S1). This transition pressure is experimentally accessible with a laser-heated diamond anvil cell. The same transition is predicted to occur at ~ 490 GPa (4) in the silicate, which is beyond the limit of current static compression techniques.

Here we have examined Mg_2GeO_4 above 160 GPa, showing that a cubic Th_3P_4 -type phase ($I\bar{4}3d$) is synthesized under such conditions. The intrinsically disordered Th_3P_4 phase is characterized by eight-fold coordination of Ge by oxygen and can be understood as the result of a thermally induced order-disorder transition of the low-temperature tetragonal phase. The ordered $I\bar{4}2d$ predicted by calculations (9) based on density functional theory (DFT) was not observed. The formation of the Th_3P_4 -type phase in the corresponding silicate at higher pressures would have important implications for the interior mineralogy of large, rocky extrasolar planets.

Results

In the first experimental run, Mg_2GeO_4 olivine was compressed in a diamond anvil cell to 179 GPa at room temperature. At this pressure, the X-ray diffraction (XRD) pattern only contained gold peaks, indicating the germanate underwent pressure-induced amorphization (10). The sample was first heated to 1255 ± 32 K and then to a peak temperature of 3232 ± 141 K in steps of ~ 150 K, with ~ 5 minutes of heating at each step. At 1255 K, four new diffraction peaks appeared and the XRD pattern remained unchanged upon further heating to 2010 ± 42 K (Fig. 1).

At higher temperature (2302 ± 65 K), additional changes in the diffraction pattern occurred. The higher temperature diffraction data are consistent with the formation of MgGeO_3 post-perovskite ($Cmcm$) (Suppl. Material, Fig. S3 and Table S1). The unit cell parameters of pPv determined from the diffraction pattern quenched to room temperature at 172 GPa are in very good agreement with previous results (11) at similar pressure. MgO ($B1, Fm\bar{3}m$) is also expected as a decomposition product of Mg_2GeO_4 , but MgO peaks overlap with gold peaks at these pressures. In the MgO-GeO_2 system, the $I\bar{4}2d$ -type Mg_2GeO_4 phase is predicted to occur at ~ 175 GPa (9). Fig. S4 of the supplementary material compares the observed XRD pattern at 187 GPa, 2010 K with the calculated pattern of tetragonal $I\bar{4}2d$ -type Mg_2GeO_4 . Although the peak splittings expected for this structure are not observed, the peak positions of the $I\bar{4}2d$ -type phase are generally similar to the observed data, suggestive of a related higher symmetry structure.

Assuming a cubic unit cell, a single indexing is possible, consistent with a body-centered-cubic lattice ($h + k + l = 2n$). Within the minimal supergroups of $I\bar{4}2d$ (#122), space group $I\bar{4}3d$ (#220) provides the only possible solution. Of ~ 40 candidate structure types for the AB_2X_4 stoichiometry (12), only one structure with this space group is known: the thorium phosphide structure (Suppl. Material, Section. S5), Th_3P_4 ($I\bar{4}3d, Z=4$). Fitting the observed diffraction data

to this structure yields a good match to the peak positions (Suppl. Material, Table. S2). The Th_3P_4 structure is commonly observed in rare Earth chalcogenides (12). The cations are in eight-fold coordination and each anion is bonded to six cations in this structure (Fig. 2). It is intrinsically disordered with both cations having partial occupancy of the $12a$ Wyckoff site (Mg: 2/3, Ge: 1/3). At high temperature, this type of disordered phase can be stabilized by configurational entropy. While this is an unexpected result given the large difference in cation valence ($\text{Mg}^{2+}/\text{Ge}^{4+}$), the energetics associated with different site occupancies across species may diminish under extreme compression.

A theoretical study has also very recently predicted this structure occurs through a high-temperature order-disorder transition of the tetragonal $I\bar{4}2d$ -type phase (13). Our results independently establish the stability of the Th_3P_4 -type phase in Mg_2GeO_4 at ultra-high pressure and temperature and provide direct experimental verification of this phase. Furthermore, there are fundamental differences (as discussed later) between the proposed and observed phase diagrams, demonstrating the importance of experimental validation.

In the second experimental run, we pressurized Mg_2GeO_4 to 162 GPa at room temperature. On heating to 1441 ± 57 K (Suppl. Material, Fig. S5a), diffraction peaks assigned to the Th_3P_4 -type phase were observed and retained on quenching to ambient temperature. The sample was then further compressed to 240 GPa and heated to a peak temperature of 3650 ± 191 K (Suppl. Material, Fig. S5b). The Th_3P_4 peaks sharpened on heating and were retained on temperature quench. All the XRD peaks in the observed pattern can be indexed using Th_3P_4 -type Mg_2GeO_4 (Suppl. Material, Table S3), Re, and Au. Figure 2 shows a Le Bail refinement of the diffraction pattern showing a good fit to the data. The corresponding two-dimensional image (Suppl. Material, Fig. S6) shows smooth diffraction rings. Further increase in pressure to 263 GPa did not lead to any

additional changes in the XRD pattern. Fig. 3 shows the temperature quenched diffraction patterns at 161 GPa, 225 GPa, and an *in situ* pattern at 275 GPa, 2023 ± 35 K.

Figure 4a summarizes the phase diagram of Mg_2GeO_4 . As mentioned above, recent DFT calculations (9) predict a transition from MgGeO_3 (pPv) and MgO to the tetragonal $I\bar{4}2d$ -type Mg_2GeO_4 at 175 GPa with a negative Clapeyron slope. Additional calculations predict a transition between $I\bar{4}2d$ -type and Th_3P_4 -type occurring above ~ 2500 K. The $I\bar{4}2d$ phase was not observed in any of our experiments, but we consistently observed the higher symmetry $I\bar{4}3d$ -type phase at all temperatures. Our results indicate that the $I\bar{4}3d$ -type Mg_2GeO_4 phase is stable as low as 162 GPa and remains stable to at least 275 GPa. Based on limited heating runs at selected temperatures, the phase boundary between pPv + MgO and $I\bar{4}3d$ Mg_2GeO_4 appears to have a positive Clapeyron slope. This is in contrast to theoretical predictions (13) of a negative Clapeyron slope of both the pPv to $I\bar{4}3d$ and pPv to $I\bar{4}2d$ phases (Fig. 4). The formation of the $I\bar{4}3d$ -type phase was also observed on heating to 1255 K at 179 GPa, which is considerably lower than the theoretically predicted transition temperature of ~ 2800 K at 175 GPa. The minimum temperature that could be measured on heating was ~ 1200 K. The fast quench rate in our experiment likely precludes a transition to the tetragonal ordered phase at low temperatures. Substitutional ordering requires site diffusion that may be kinetically limited at multi-Mbar pressures. Further work will be necessary to better constrain the extent of stability of the Th_3P_4 -type phase at lower temperatures.

Figure 4b compares the densities of phases in the MgO-GeO₂ system. The densities of MgGeO_3 + MgO mixtures were calculated assuming an ideal solid solution (i.e., the molar volumes are additive). The density of the mixture (ρ) is given by:

$$\frac{1}{\rho(P, T)} = \frac{(1 - m_2)}{\rho_1(P, T)} + \frac{m_2}{\rho_2(P, T)},$$

where m and ρ are the mass fraction and density of the individual components. Our results indicate that the transition from post-perovskite and MgO to the Th_3P_4 -type phase produces a relatively large (3.3%) change in density at 160 GPa.

Discussion

Changes in silicon coordination in minerals can influence the structure and dynamics of planetary interiors. The transition in silicates from tetrahedral (four-fold) to octahedral (six-fold) coordination of silicon by oxygen occurring near 660-km depth defines the major structural boundary in Earth's mantle (14). Changes in key physical and chemical properties such as density, rheology, and element partitioning occur together with the coordination change. In Earth, six-coordinated silicate phases are expected to be stable throughout the lower mantle with (Mg, Fe) SiO_3 post-perovskite and SiO_2 seifertite (α - PbO_2 -type, $Pbcn$) stable at core-mantle boundary conditions (~ 135 GPa). In the case of SiO_2 , a further transition to the pyrite-type phase ($Pa\bar{3}$) is observed at 268 GPa (15), but this phase retains 6-fold coordination (sometimes described as 6 + 2). Increases in coordination above six have been reported in SiO_2 glass at ultra-high pressures (16). However, there is no experimental evidence for silicon coordination greater than six in any high-pressure crystalline silicates or their analogues.

While pPv MgSiO_3 is the expected silicate phase at the base of Earth's mantle, post-pPv phases with Si-O coordination > 6 may play a decisive role in terrestrial super-Earths of four or greater Earth masses (Fig. S1). If the Th_3P_4 -type phase also exists in Mg_2SiO_4 , the change in coordination from 6-fold to 8-fold may be accompanied by major changes in physical, chemical, and thermodynamic properties. The $\sim 3\%$ density change ($\Delta\rho$) associated with the transition is large ($\Delta\rho = \sim 1.5\%$ for Pv to pPv) for ultra-high pressure phase transitions and may affect the dynamic behavior of the deep mantle.

The Th_3P_4 -type phase is related to the tetragonal $I\bar{4}2d$ structure by an order-disorder transition across cation sites. The expected high internal temperatures of super-Earth mantles (Suppl. Material, Fig. S1) will likely favor the Th_3P_4 -type phase over the $I\bar{4}2d$ structure. The intrinsically disordered nature (Suppl. Material, Section S5) of the Th_3P_4 -type phase may also be an important feature as it suggests enhanced miscibility of chemical components at ultrahigh P-T conditions. Among chalcogenides, Th_3P_4 -type phases are noted for their flexible structure and prevalence of defects, impurities, and disorder (17). This structural flexibility can affect rheology and transport properties. Compared to other structures, enhanced phonon scattering in this disordered phase may yield an anomalously low thermal conductivity (18). Based on the calculated 0-K transition pressure from pPv to the ordered $I\bar{4}2d$ phase, it is expected that a transition to the Th_3P_4 -type phase may result in important differences in mantle structure and deep dynamics in planets above and below four Earth masses in size.

In summary, we have synthesized Mg_2GeO_4 in the thorium phosphide structure above 160 GPa. The phase is calculated to be $\sim 3\%$ denser than the mixture of MgGeO_3 post-perovskite and MgO . This is the first experimental synthesis of a phase with Ge in eight-fold coordination with oxygen and the first occurrence of the Th_3P_4 -type phase in an oxide. Just as the discovery of widespread six-coordinated germanates/silicates profoundly altered our understanding of silicate crystal chemistry and its role in the Earth's deep interior, the discovery of an eight-fold coordinated, intrinsically disordered germanate opens the possibility of previously unexplored crystal-chemical behavior in the silicate minerals of large rocky exoplanets. Our results also raise the possibility that this structure or the related $I\bar{4}2d$ structure could also be adopted by other oxide minerals at extreme pressures. Thus, our results suggest the possibility of novel crystal chemistry in A_3O_4 - and AB_2O_4 -type compounds that warrant further exploration.

Acknowledgments

We acknowledge helpful discussions with Ronald Cohen and Kai Luo. We are also grateful to Peng Ni for his assistance with sample synthesis. This research was supported by the National Science Foundation (NSF) – Earth Sciences (EAR-1836852). RD is grateful for support from the Carnegie Endowment. We acknowledge the support of GeoSoilEnviroCARS (Sector 13), which is supported by the NSF - Earth Sciences (EAR-1128799), and the U.S. Department of Energy (DOE), Geosciences (DE-FG02-94ER14466). This research used resources of the Advanced Photon Source, a DOE Office of Science User Facility operated by Argonne National Laboratory under Contract No. DE-AC02-06CH11357.

References

1. T. V. Hoolst *et al.*, *Adv. Phys: X*, **4**, 1630316 (2019).
2. K. Umemoto, R. M. Wentzcovitch, *Earth Planet. Sci. Lett.* **311**, 225–229 (2011).
3. T. S. Duffy *et al.* in *Treatise on Geophysics (2nd Ed.)*, G. Schubert, Ed. (Elsevier, Oxford, ed. 2nd, 2015), pp. 149–178.
4. K. Umemoto *et al.*, *Earth Planet. Sci. Lett.* **478**, 40–45 (2017).
5. M. H. Shahnas *et al.*, *J. Geophys. Res: Planets*. **123**, 2162–2177 (2018).
6. A. E. Ringwood, M. Seabrook, *J. Geophys. Res.* **68**, 4601–4609 (1963).
7. C. V. Stan *et al.*, *Inorg. Chemistry*. **56**, 8026–8035 (2017).
8. K. Hirose *et al.*, *Am. Min.* **90**, 262–265 (2005).
9. K. Umemoto, R. M. Wentzcovitch, *Phys. Rev. Materials*. **3**, 123601 (2019).
10. T. Nagai *et al.*, *Miner. J. Japan*. **17**, 151–157 (1994).
11. A. Kubo *et al.*, *Geophys. Res. Lett.* **33** L12S12 (2006).
12. X. Zhang *et al.*, *Phys. Rev. B*. **86**, 014109 (2012).
13. K. Umemoto, R. M. Wentzcovitch, *arXiv:2012.08056 [cond-mat]* (2020).
14. T. Irifune, A. *Earth Planet. Sci. Lett.* **117**, 101–110 (1993).

15. Y. Kuwayama *et al.*, *Science*. **309**, 923–925 (2005).
16. C. Prescher *et al.*, *Proc. Natl. Acad. Sci. U. S. A.* **114**, 10041–10046 (2017).
17. C. E. Whiting *et al.*, in *2018 IEEE Aero. Conf.* 1–9 (2018).
18. G. J. Snyder, E. S. Toberer, in *Materials for Sustainable Energy* (Macmillan Publishers Ltd, UK, 2010; pp. 101–110).
19. K. Hirose *et al.*, *Am. Min.* **90**, 262–265 (2005)).
20. C. E. Runge *et al.*, *Phys. Chem. Miner.* **33**, 699–709 (2006).
21. L. Liu, in *High-Pressure Research*, M. H. Manghnani, S.-I. Akimoto, Eds. (Academic Press, 1977, pp. 245–253).
22. A. Schubnel *et al.*, *Science*. **341**, 1377–1380 (2013).
23. Y. Meng *et al.*, *Phys. Chem. Miner.* **21**, 407–412 (1994).
24. P. E. Petit *et al.*, *Phys. Chem Miner.* **23**, 173–185 (1996).
25. S. Speziale *et al.*, *J. Geophys. Res: Solid Earth.* **106**, 515–528 (2001).
26. S. D. Jacobsen *et al.*, *Am. Min.* **93**, 1823–1828 (2008).

Fig. 1. X-ray diffraction patterns before (black) and during heating (purple and red) of Mg_2GeO_4 at 179 GPa. The asterisks and diamonds represent the peaks appearing at lower and higher temperatures, respectively.

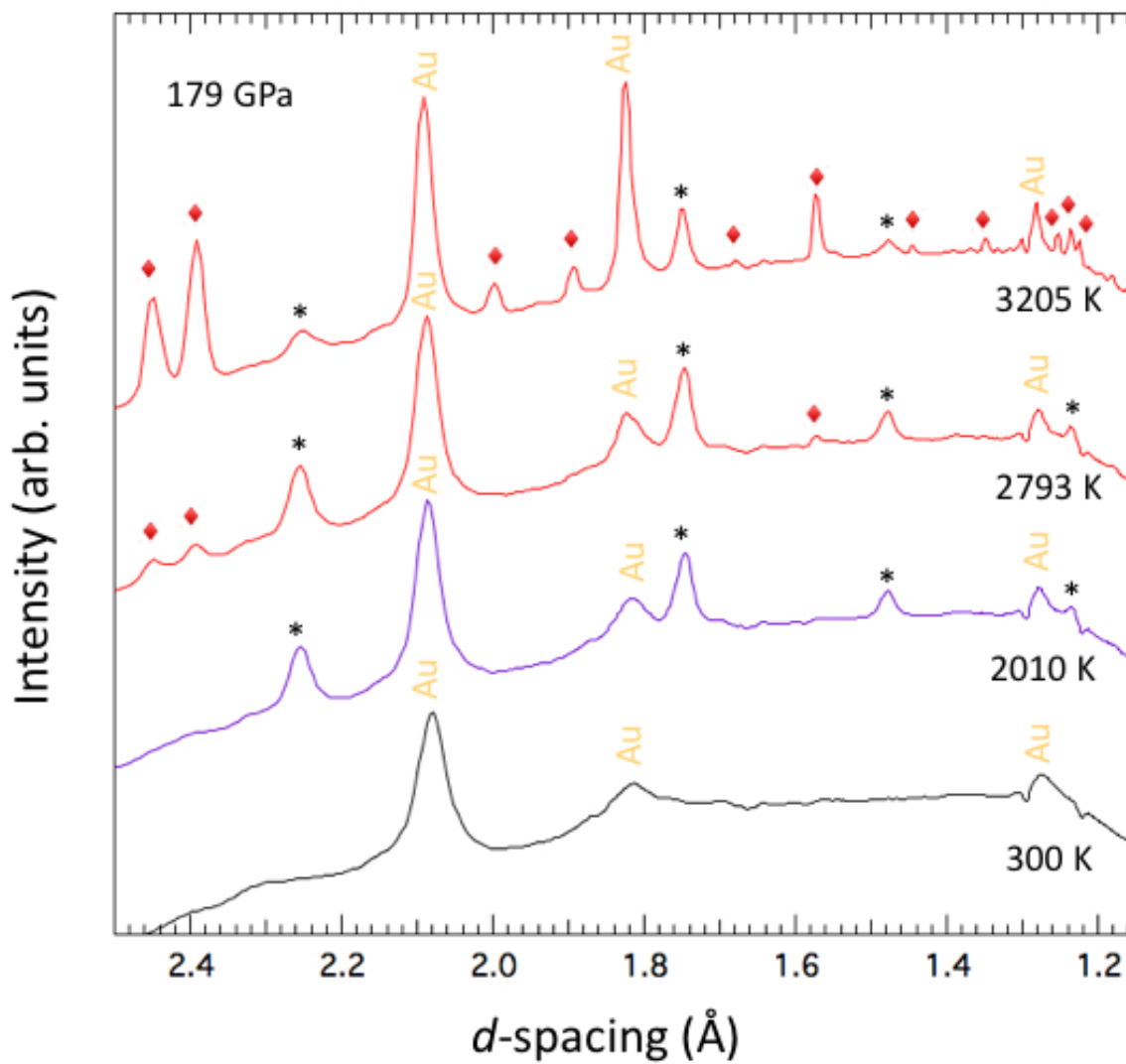


Fig. 2. (a) Le Bail refinement of the X-ray diffraction pattern (black) obtained after heating Mg_2GeO_4 to 3650 K at 240 GPa with subsequent quenching to room temperature. Red and green curves show the fit and background, respectively. Miller indices of the Th_3P_4 -type Mg_2GeO_4 are shown above the observed diffraction pattern. (b) Structure of the Th_3P_4 -type phase: Red spheres are oxygen atoms and orange/mauve spheres represent the Mg/Ge site with shading to indicate 2/3 occupancy by Mg and 1/3 occupancy by Ge. A representative (Mg, Ge) O_8 polyhedron is also shown.

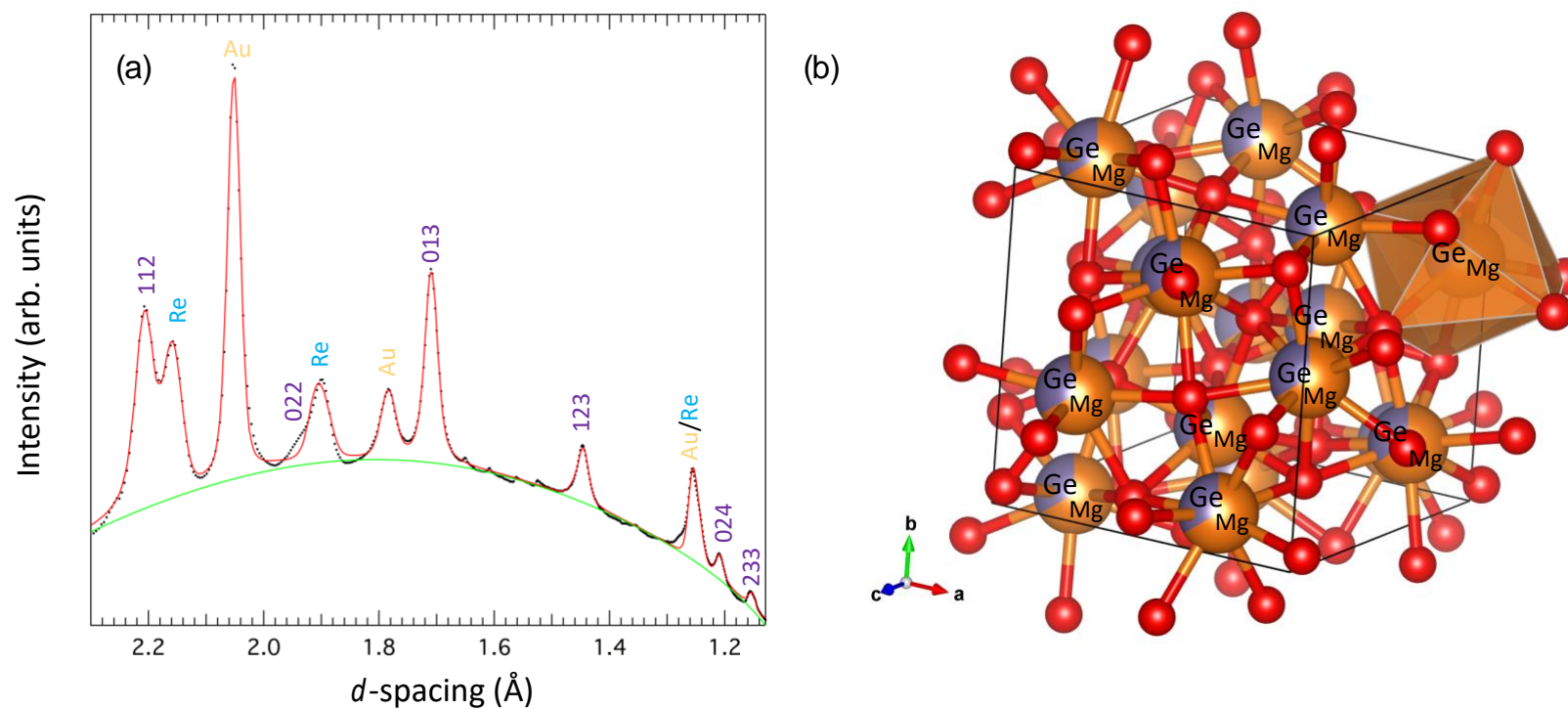


Fig. 3. X-ray diffraction patterns of the Th₃P₄-type phase of Mg₂GeO₄ at 161 GPa, 225 GPa, and 275 GPa. The two lower pressure patterns are collected at quenched temperatures (300 K) whereas the upper pattern was collected at 2020 K. Th₃P₄-type, Au, and Re peaks are indicated with Miller indices.

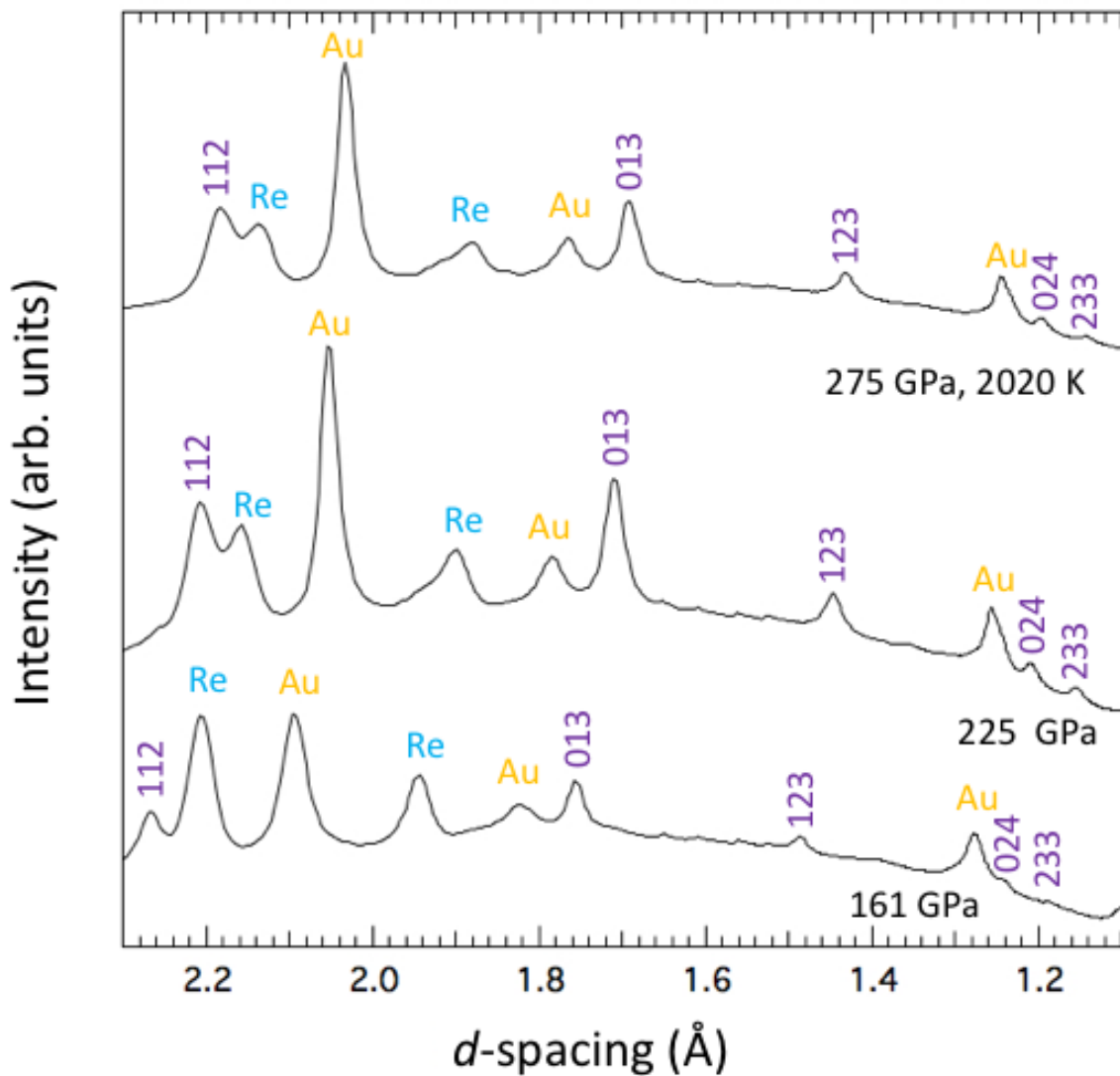
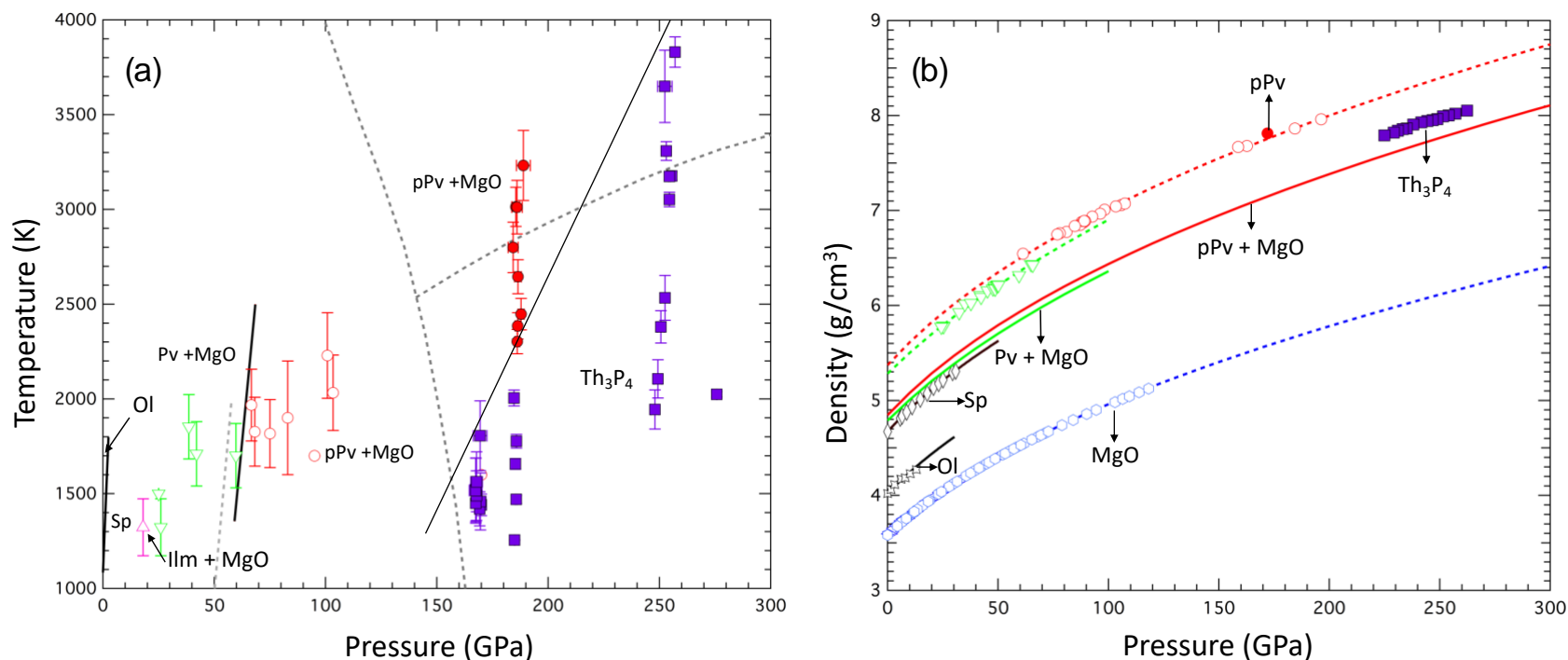


Fig. 4 (a) Phase diagram of Mg_2GeO_4 . Solid symbols (red circles: pPv; purple squares: Th_3P_4) are from the present study. The open symbols indicate previous work (red circles: pPv (11, 19); green inverted triangles: Pv (19–21); pink triangle: ilmenite (Ilm) + MgO (21)). The solid black lines represent phase boundaries, from left: Olivine (Ol)→Spinel (Sp) (22), Pv→pPv (19), pPv + MgO→ Th_3P_4 (this study). Dashed grey lines indicate theoretical calculations: Pv + MgO→pPv + MgO, pPv + MgO→ $I\bar{4}2d$ Mg_2GeO_4 , pPv + MgO→ Th_3P_4 -type Mg_2GeO_4 (9, 13). The solid black line is a guide to the eye for the pPv + MgO→ $I\bar{4}3d$ Mg_2GeO_4 from this work. **(b)** Densities of selected phases in the MgO-GeO₂ system. Solid (this work) and open (previous studies) symbols represent 300-K experimental data: red circles: pPv (11); green triangles: Pv (20); brown diamonds: spinel (23); black stars: olivine (24); blue hexagons: B1-MgO (25, 26). Colored dashed (MgGeO_3) and solid lines (Mg_2GeO_4) are 3rd order Birch-Murnaghan equation fits to the respective data sets. The red and green solid lines are the calculated densities of mixtures of MgGeO_3 Pv and pPv with MgO.



Supplementary Material

Ultra-high pressure disordered eight-coordinated phase of Mg₂GeO₄: Analogue for super-Earth mantles

R. Dutta^{1,2*}, S. J. Tracy¹, J. Yang¹, P. C. Burnley³, D. Smith⁴, Y. Meng⁴, S. Chariton⁵, V. B. Prakapenka⁵, and T. S. Duffy²

¹Earth and Planets Laboratory, Carnegie Institution for Science, Washington DC 20015 USA.

²Department of Geosciences, Princeton University, Princeton, NJ 08540 USA.

³Department of Geoscience, University of Nevada, Las Vegas, NV 89154 USA.

⁴HPCAT, Advanced Photon Source, Argonne National Laboratory, Argonne, IL 60439 USA

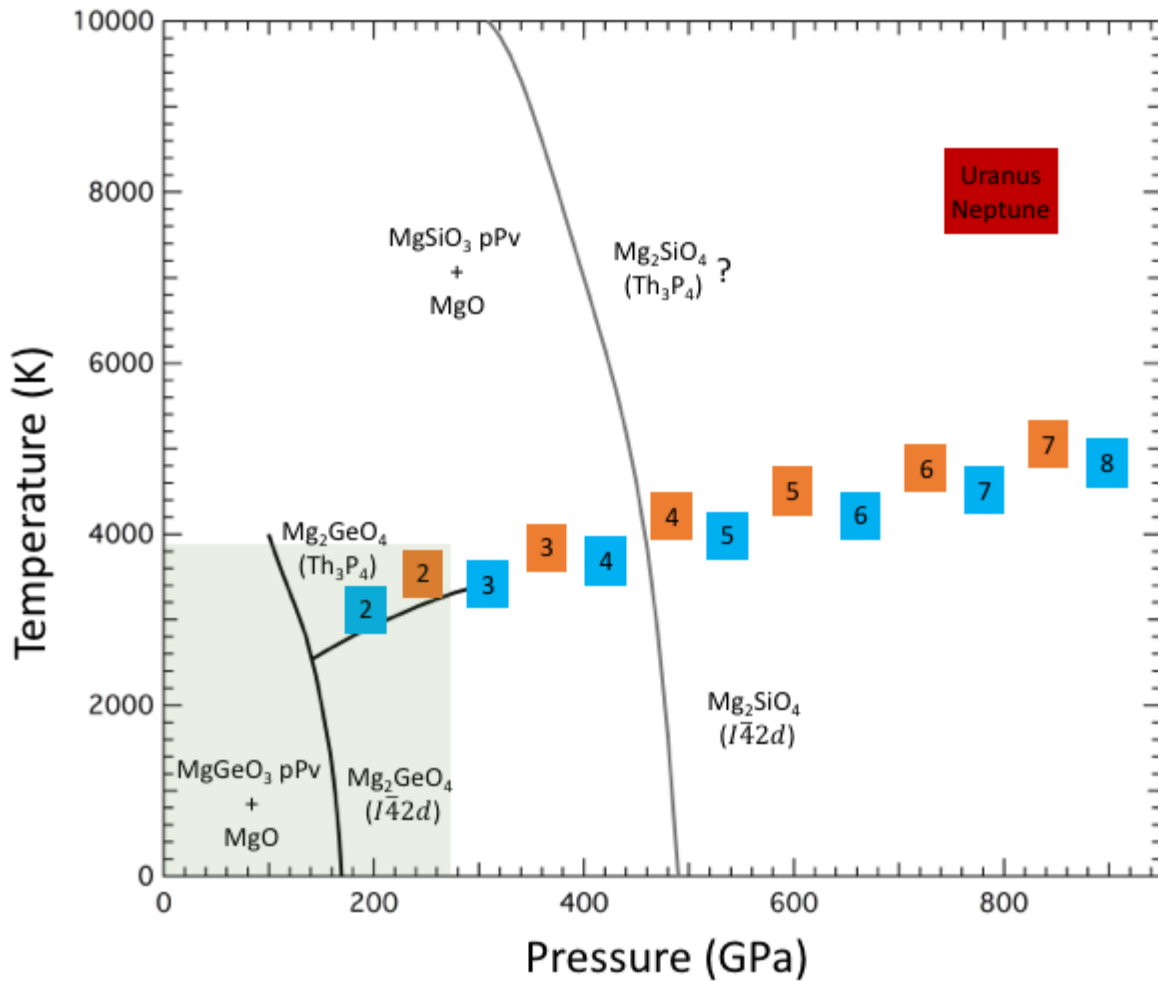
⁵Center for Advanced Radiation Sources, University of Chicago, Chicago, IL 60637 USA.

Contents

- S1. Predicted phase boundaries for Mg_2GeO_4 and Mg_2SiO_4 at multi-megabar pressures
- S2. Experimental methodology
- S3. X-ray diffraction data for Mg_2GeO_4 post-perovskite
- S4. Comparison with $I\bar{4}2d$ -type Mg_2GeO_4
- S5. Structure and crystal chemistry of the thorium phosphide-type phase
- S6. Supplemental X-ray diffraction results for the Th_3P_4 -type phase of Mg_2GeO_4

S1. Predicted phase boundaries for Mg_2GeO_4 and Mg_2SiO_4 at multi-megabar pressures

Fig. S1. Calculated phase boundaries (1, 2) for Mg_2SiO_4 (grey solid line) and Mg_2GeO_4 (black solid line). Orange and blue squares show the pressure-temperature conditions expected at the core-mantle boundaries of terrestrial- and water-rich exoplanets, respectively (3). The numbers in each square represent the mass of the planet as a multiple of Earth's mass. The shaded region represents the P, T range of this study. The question mark indicates the possible stability of Th_3P_4 -type Mg_2SiO_4 .



S2. Experimental methodology

Mg₂GeO₄ olivine samples were synthesized according to established procedures (4, 5) and confirmed by X-ray diffraction. The sample was mixed with 10 wt.% gold which acted as a pressure calibrant and laser absorber. Rhenium gaskets were pre-indented and ~20 μm diameter holes were laser drilled to form the sample chamber in a diamond anvil cell. The sample + Au pellets were then loaded into a cell with beveled 50-μm culet anvils (Fig. S2). No pressure medium was used in order to maximize the X-ray diffraction signal from the sample.

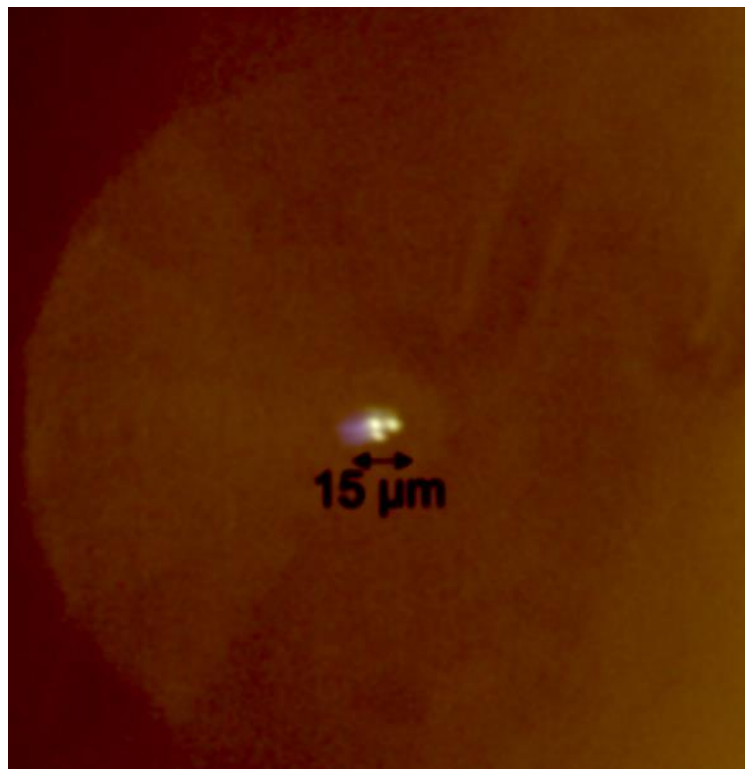
Angle-dispersive X-ray diffraction was carried out at 13-ID-D and 16-ID-B of the Advanced Photon Source using monochromatic X-rays ($\lambda = 0.3344 \text{ \AA}$ and 0.4066 \AA , respectively) focused to dimensions of $3 \times 3 \text{ \mu m}^2$ and $5 \times 3 \text{ \mu m}^2$, respectively. CdTe 1M Pilatus detectors were used to collect the diffraction patterns. LaB₆ and CeO₂ standards were used to calibrate the detector position and orientation.

High temperatures were attained by double-sided heating with diode pumped fiber lasers with ~10-15 μm spot sizes. Temperature was increased in a stepwise fashion with ~150-200 K steps with a heating duration of 2-5 minutes at each step. The laser power was adjusted independently on both sides to keep temperature differences to < 150 K. Temperatures were measured using spectroradiometry. Pressure was determined using the (111) reflection of Au (6). Thermal pressures were accounted for using the Mie-Grüneisen equation of state.

The two-dimensional X-ray diffraction images were integrated to one-dimensional patterns using DIOPTAS (7) and fit using background-subtracted Voigt line shapes. Lattice parameters were calculated by least-squares refinement of the peak positions (8) or whole profile Le Bail refinement as implemented in MAUD (9). For the whole pattern refinement, the

background was fit with a 4th order polynomial, instrumental profile terms were fit with Gaussian Cagliotti terms and sample broadening incorporated isotropic size and strain broadening.

Fig. S2. A typical loaded diamond anvil cell at 78 GPa.



S3. X-ray diffraction data for Mg₂GeO₄ post-Perovskite

Fig. S3. X-ray diffraction pattern obtained after heating Mg₂GeO₄ to 3200 K at 179 GPa, followed by quenching to room temperature (quenched P = 172 GPa). The tick marks at the bottom indicate the expected peak positions for post-perovskite (red), gold (yellow), and MgO (blue). Miller indices of pPv- (red) and Th₃P₄-type (purple) Mg₂GeO₄ (purple) are listed above each peak.

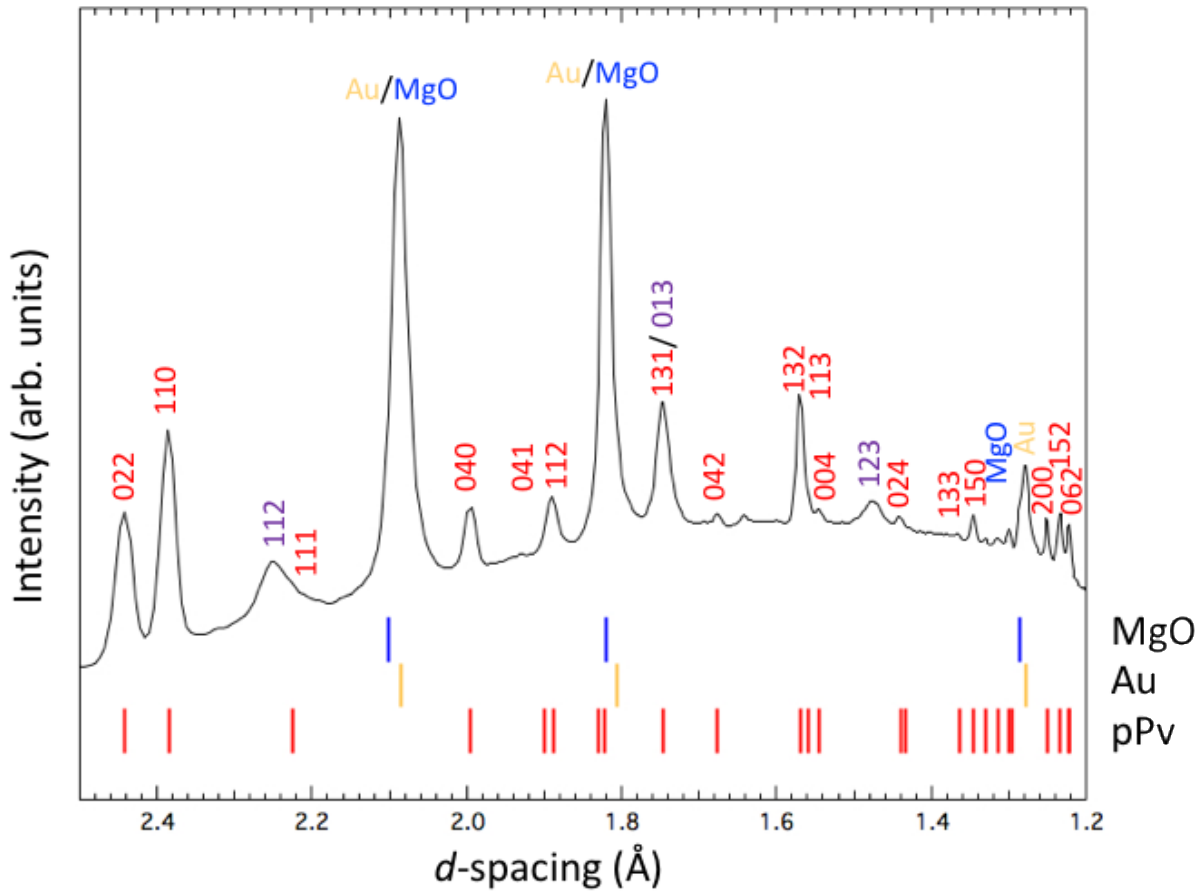
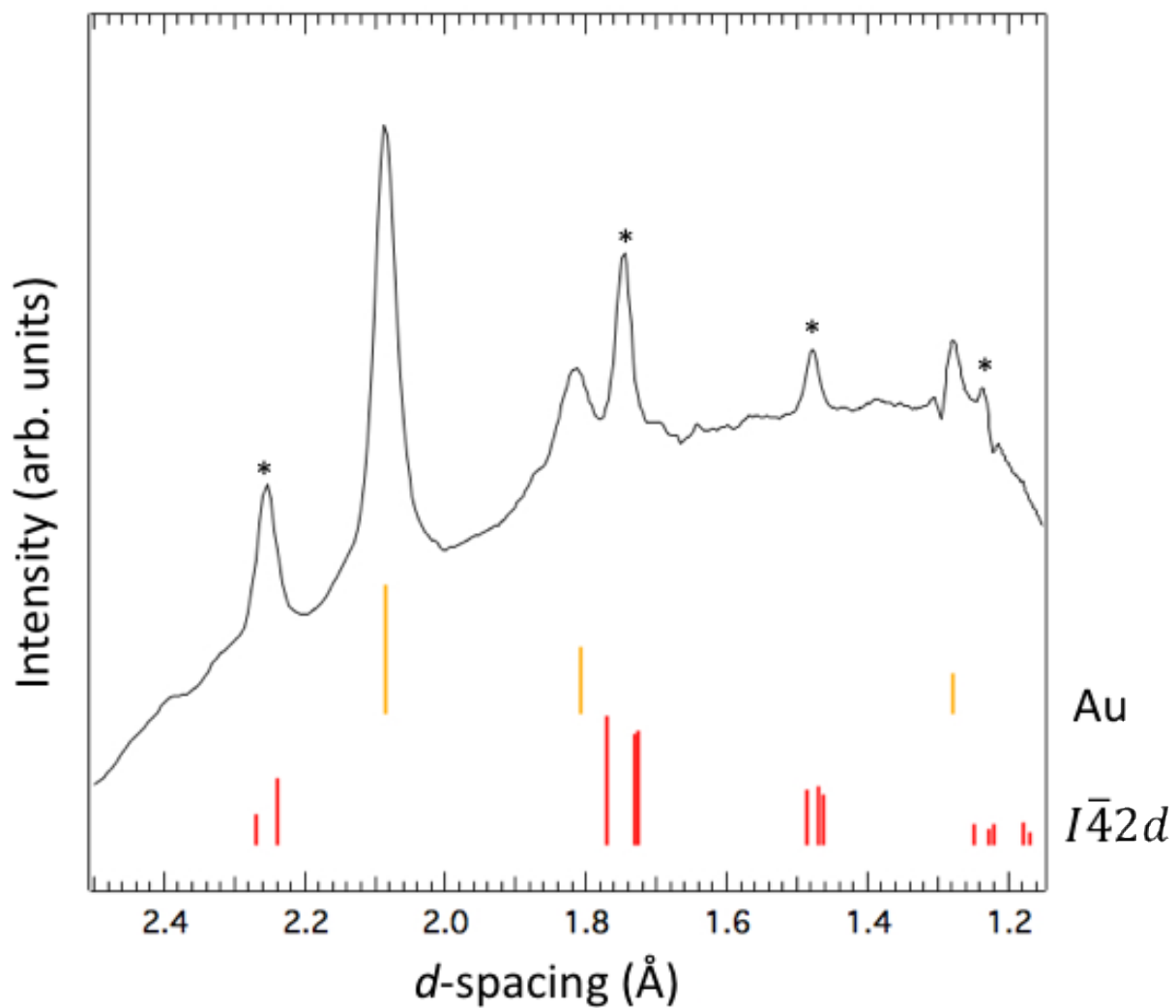


Table S1. Calculated and observed d -spacings of post-perovskite Mg_2GeO_4 at 172 GPa. The fit lattice parameters are $a = 2.498$ (1) Å, $b = 7.982$ (3) Å, and $c = 6.177$ (4) Å.

h	k	l	d -observed (Å)	d -calculated (Å)	Δd (Å)
0	2	0	3.9905	3.9911	-0.0006
0	0	2	3.0869	3.0883	-0.0014
0	2	2	2.4431	2.4425	0.0006
1	1	0	2.3851	2.3847	0.0004
0	4	0	1.9956	1.9955	0.0001
1	3	1	1.7462	1.7471	-0.0009
1	3	2	1.5694	1.5689	0.0005

S4. Comparison with $I\bar{4}2d$ -type Mg_2GeO_4

Fig. S4. Comparison of the observed diffraction pattern at 187 GPa, 2010 K with the theoretically proposed $I\bar{4}2d$ -type Mg_2GeO_4 structure ($I0$) ($a = 5.474 \text{ \AA}$, $c = 5.656 \text{ \AA}$ at 150 GPa).



S5. Structure and crystal chemistry of the thorium phosphide-type phase

The Th_3P_4 structure was originally described by Meisel (1939) (11) and Kripyakevich (1963) (12). It is based on a body-centered-cubic lattice with the cations in eight-fold coordination. The Mg and Ge ions occupy site $12a$, while the oxygens are located on site $16c$. Thus, the structure is intrinsically disordered with both cations occupying the same crystallographic site. There is a single positional parameter, x . The nearest-neighbor cation-anion bond distances are identical when x adopts its ideal value, $1/12$. The cation polyhedra are in the form of a strongly distorted cube (octaverticon) with triangular faces. Each anion is bonded to six cations in a distorted octahedron.

The Th_3P_4 -type structure occurs commonly in binary chalcogenides of the light rare earth elements in both defective (A_2X_3) and non-defective forms (A_3X_4), often exhibiting solid solutions between them (13). It also occurs widely in ternary AB_2X_4 chalcogenides where A is a divalent metal cation and B is a light rare earth element (14, 15). Its prevalence in light rare earths indicate the structure is favored by compounds with a large ratio of cation to anion radius. Based on AB_2X_4 structure maps (14, 15), the phase is restricted to compounds in which the radii of the cations, r_A and r_B , are similar ($r_A/r_B \sim 0.8 - 1.2$) and have low electronegativity. At larger cation radius ratios, the calcium ferrite-type structure (CaFe_2O_4) is preferred instead. Chalcogenides with the Th_3P_4 structure have attracted interest for technical applications because the structure is highly flexible and can incorporate many types of impurities and defects (16).

At high pressures and temperatures, ternary sulfospinel AB_2S_4 (A=Mg, Mn, B=Tm, Yb) have been shown to transform to the Th_3P_4 -type structure (17). The structure has also been synthesized at high pressure in nitrides including Hf_3N_4 , Zr_3N_4 , and Ti_3N_4 , in which the phase is

found to be highly incompressible (18, 19). The structure can also describe an electride phase in alkali metals formed at high pressure (20).

S6. Supplemental X-Ray diffraction results for the Th₃P₄-type phase of Mg₂GeO₄

Table S2. Calculated and observed d -spacings of Th₃P₄-type Mg₂GeO₄ at 187 GPa and 2010 K.

The lattice parameter is $a = 5.523$ (1) Å.

h	k	l	d -observed (Å)	d -calculated (Å)	Δd (Å)
1	1	2	2.2549	2.2546	0.0003
0	1	3	1.7466	1.7464	0.0002
1	2	3	1.4780	1.4759	0.0021
0	2	4	1.2335	1.2349	-0.0014

Table S3. Calculated and observed d -spacings of Th₃P₄-type Mg₂GeO₄ obtained after heating to 3650 K at 240 GPa and then quenching to room temperature. The lattice parameter is $a = 5.4055$

(7) Å. The unit cell dimension is in excellent agreement with that obtained from a Le Bail refinement of the same pattern, $a = 5.4055$ (2) Å.

h	k	l	d -observed (Å)	d -calculated (Å)	Δd (Å)
1	1	2	2.2064	2.2068	-0.0004
0	1	3	1.7090	1.7093	-0.0003
1	2	3	1.4462	1.4446	0.0016
0	2	4	1.2079	1.2087	-0.0008
2	3	3	1.1525	1.1524	0.0001

Fig. S5. X-ray diffraction pattern before and during heating Mg_2GeO_4 to ~ 1810 K at 162 GPa (a) and ~ 3650 K at 240 GPa (b). The ticks at the bottom indicate the peaks from Th_3P_4 -type Mg_2GeO_4 (purple), gold (yellow), and rhenium (light blue). Miller indices of the Th_3P_4 -type phase have been listed above the observed pattern.

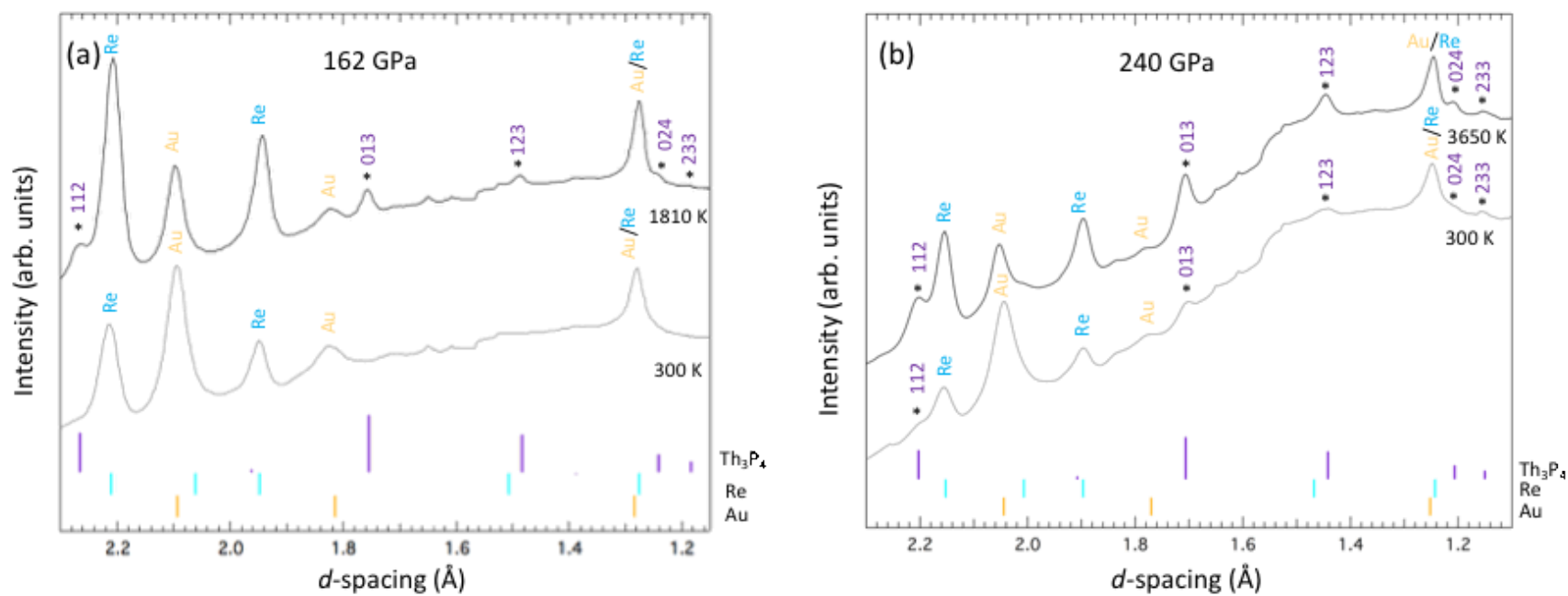
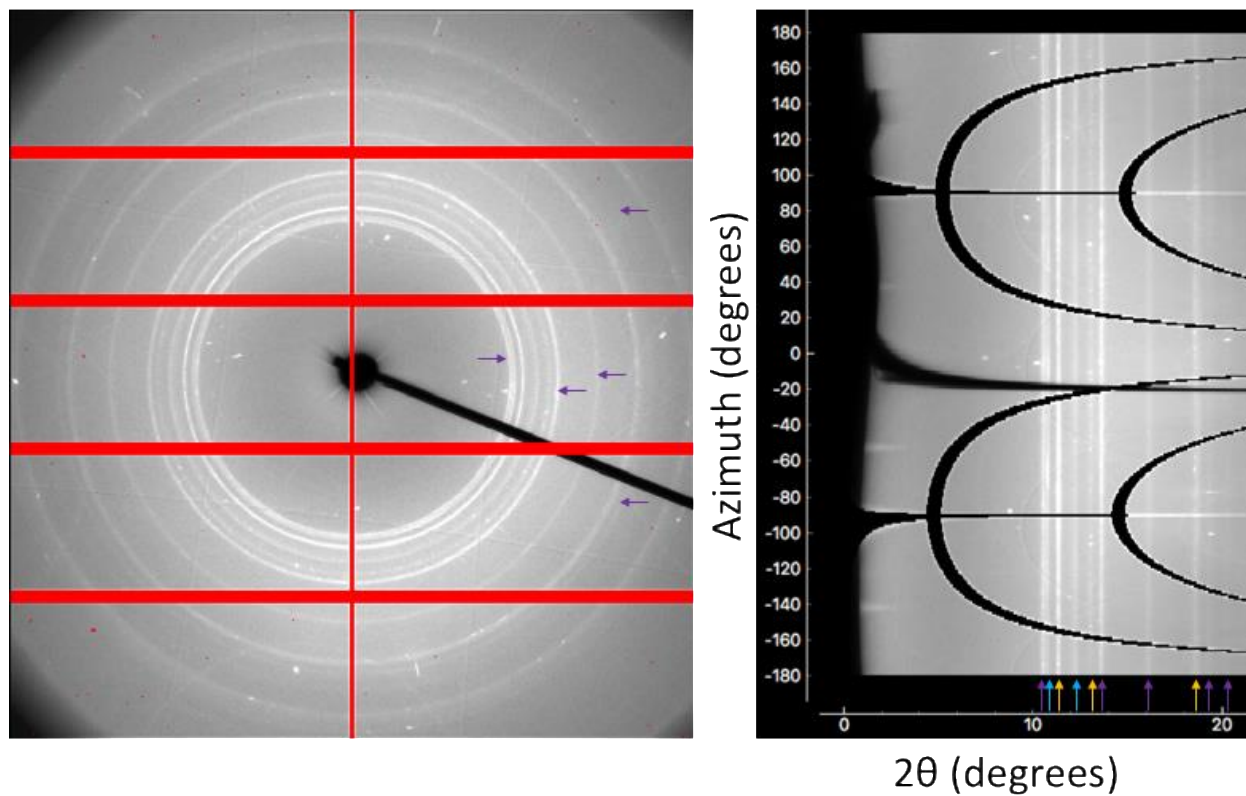


Fig. S6. Two-dimensional diffraction pattern of Mg_2GeO_4 after heating to 3650 K at 240 GPa with subsequent quenching to room temperature. The left figure shows the raw image, which is transformed to coordinates of azimuthal angle around the X-ray beam vs. two-theta in the right-hand image. The integrated one-dimensional pattern for this image is shown in Fig. 2. Arrows (yellow: Au, light blue: Re, and purple: Th_3P_4 -type Mg_2GeO_4) show the peaks positions in the integrated pattern.



References

1. K. Umemoto *et al.*, *Earth. Planet. Sci. Lett.* **478**, 40–45 (2017).
2. K. Umemoto, R. M. Wentzcovitch, *arXiv:2012.08056 [cond-mat]* (2020)
3. C. Sotin *et al.*, *Icarus*. **191**, 337–351 (2007).
4. R. B. Von Dreele *et al.*, *Acta Cryst B*. **33**, 2287–2288 (1977).
5. P. C. Burnley, Ph.D Thesis, University of California- Davis (1990).
6. Y. Fei *et al.*, *Proc. Natl. Acad. Sci. U.S.A.* **104**, 9182–9186 (2007).
7. C. Prescher *et al.*, *High. Press. Res.* **35**, 223–230 (2015).
8. T. J. B. Holland, S. A. T. Redfern, *Mineral. Mag.* **61**, 65–77 (1997).
9. L. Lutterotti, *Nucl. Instrum. Methods Phys. Res. B*. **268**, 334–340 (2010).
10. K. Umemoto, R. M. Wentzcovitch (*Personal Communication*).
11. K. Meisel, *Z. anorg. allgem. Chem.* **240** (1939).
12. P. I. Kripyakevich, *Soviet. Phys. Cryst.* **7** (1963).
13. J. Flahaut *et al.*, *Acta Cryst.* **19**, 14–19 (1965).
14. X. Zhang, A. Zunger, *Adv. Funct. Mater.* **20**, 1944–1952 (2010).
15. J. E. Iglesias, H. Steinfink, *J. Solid State Chem.* **6**, 119–125 (1973).
16. C. E. Whiting *et al.*, in *2018 IEEE Aero. Conf.* 1–9 (2018).
17. K. Hirota *et al.*, *Mater. Res. Bull.* **11**, 227–232 (1976).
18. A. Zerr *et al.*, *Nat. Mater.* **2**, 185–189 (2003).
19. V. S. Bhadram *et al.*, *Phys. Rev. Mater.* **2**, 011602 (2018).
20. C. J. Pickard, R. J. Needs, *Phys. Rev. Lett.* **107**, 087201 (2011).